Self-Assembly of Peptide Nanotubes in an Organic Solvent

M. J. Krysmann, V. Castelletto, J. E. McKendrick, L. A. Clifton, and I. W. Hamley*

Department of Chemistry, University of Reading, Reading RG6 6AD, U.K.

P. J. F. Harris

Centre for Advanced Microscopy, University of Reading, Reading RG6 6AF, U.K.

S. M. King

Rutherford Appleton Laboratory, Chilton, Didcot, Oxon OX11 0QX, U.K.

Received March 26, 2008. Revised Manuscript Received May 1, 2008

The self-assembly of a modified fragment of the amyloid β peptide, based on sequence Aβ(16−20), KLVFF, extended to give AAKLVFF is studied in methanol. Self-assembly into peptide nanotubes is observed, as confirmed by electron microscopy and small-angle X-ray scattering. The secondary structure of the peptide is probed by FTIR and circular dichroism, and UV/visible spectroscopy provides evidence for the important role of aromatic interactions between phenylalanine residues in driving β-sheet self-assembly. The β-sheets wrap helically to form the nanotubes, the nanotube wall comprising four wrapped β-sheets. At higher concentration, the peptide nanotubes form a nematic phase that exhibits spontaneous flow alignment as observed by small-angle neutron scattering.

1. Introduction

The self-assembly of peptides into amyloid fibrils is attracting immense attention due to its relevance to amyloid diseases[1–3] and also due to the in vivo nondisease related functional roles that may be played by peptide fibrils.[4] Peptide fibrils are generally built from β-sheets, and these may twist into ribbons and tapes and even curl up completely into hollow nanotubes.

The formation of nanotubes by peptides has recently been reviewed.[5–7] They were first reported by Ghadiri et al. for stacked cyclic peptides comprising alternating D- and L- amino acids.[8] Lynn and co-workers have previously observed nanotube formation for Aβ(16−22), with capped termini CH_3CO-KLVF-FAE-NH_2 in a pH 2 aqueous solution of acetonitrile/0.1% TFA.[9] They have not reported nematic phase formation. The octapeptide lanreotide, which acts as a growth hormone inhibitor, is also known to form nanotubes based on stacked β-hairpins.[10] Peptide nanotubes have also been observed for diphenylalanine;[11,12] however, there is controversy as to whether the self-assembly of this simple dipeptide is relevant to that of longer peptides, in particular whether a normal β-sheet secondary structure can form.[13] The orientation of FF peptide tubes in a magnetic field has recently been reported.[14] Nematic phase formation has been observed for natural (hen lysozyme) amyloid fibrils[15] as well as de novo designed short peptides.[16] Nematic liquid crystalline ordering of NH_2-FF-COOH nanowires (not nanotubes) in CS_2 has recently been discussed.[17] Here, we present the first report on nematic phase formation by peptide nanotubes, using a motif based on an amyloid β-peptide sequence.

We have recently commenced a program to investigate the self-assembly of peptides based on a core sequence of the amyloid β-peptide. The amyloid β peptide is important in Alzheimer's disease, a so-called amyloid disease, and is cleaved in vivo from a larger precursor protein to form fragments with 39−43 residues.[7,18,19] We have focused on the sequence KLVFF, corresponding to Aβ(16−20). This core sequence of the amyloid β peptide is believed to be critical in aggregation of Aβ into fibrils, as indicated by several studies reviewed elsewhere.[7,20] We have examined its self-assembly in aqueous solution,[20] due to controversy as to whether it forms β-sheet fibrils or not. We found clear evidence from in situ cryo-TEM (transmission electron microscopy) and small-angle X-ray scattering experiments that it does fibrillize, and FTIR spectroscopy and fiber X-ray diffraction confirm the β-sheet structure (we discuss in detail the effects of drying during sample preparation).[20] This sample also forms hydrogels in more concentrated solution.

* Corresponding author. E-mail: I.W.Hamley@reading.ac.uk.

(1) Teplow, D. B. *Amyloid: Int. J. Exp. Clin. Invest.* **1998**, *5*, 121–142.
(2) Goedert, M.; Spillantini, M. G. *Science* **2006**, *314*, 777–781.
(3) Roberson, E. D.; Mucke, L. *Science* **2006**, *314*, 781–784.
(4) Knowles, T. P.; Fitzpatrick, A. W.; Meehan, S.; Mott, H. R.; Vendruscolo, M.; Dobson, C. M.; Welland, M. E. *Science* **2007**, *318*, 1900–1903.
(5) Reches, M.; Gazit, E. *Isr. J. Chem.* **2005**, *45*, 363–371.
(6) Gao, X.; Matsui, H. *Adv. Mater.* **2005**, *17*, 2037–2050.
(7) Hamley, I. W. *Angew. Chem., Int. Ed.* **2007**, *46*, 8128–8147.
(8) Ghadiri, M. R.; Granja, J. R.; Milligan, R. A.; McRee, D. E.; Khazanovich, N. *Nature* **1993**, *366*, 324–327.
(9) Lu, K.; Jacob, J.; Thiyagarajan, P.; Conticello, V. P.; Lynn, D. G. *J. Am. Chem. Soc.* **2003**, *125*, 6391–6393.
(10) Valery, C.; Paternostre, M.; Robert, B.; Gulik-Krzywicki, T.; Narayanan, T.; Dedieu, J. C.; Keller, G.; Torres, M. L.; Cherif-Cheikh, R.; Calvo, P.; Artzner, F. *Proc. Natl. Acad. Sci. U.S.A.* **2003**, *100*, 10258–10262.
(11) Görbitz, C. H. *Chem.-Eur. J.* **2001**, *7*, 5153–5159.
(12) Reches, M.; Gazit, E. *Science* **2003**, *300*, 625–627.
(13) Görbitz, C. H. *Chem. Commun.* **2006**, 2332–2334.
(14) Hill, R. J. A.; Sedman, V. L.; Allen, S.; Williams, P. M.; Paoli, M.; Adler-Abramovich, L.; Eaves, L.; Tendler, S. J. B. *Adv. Mater. (Weinheim, Fed. Repub. Ger.)* **2007**, *19*, 4474–4479.
(15) Corrigan, A. M.; Müller, C.; Krebs, M. R. H. *J. Am. Chem. Soc.* **2006**, *128*, 14740–14741.
(16) Aggeli, A.; Nyrkova, I. A.; Bell, M.; Harding, R.; Carrick, L.; McLeish, T. C. B.; Semenov, A. N.; Boden, N. *Proc. Natl. Acad. Sci. U.S.A.* **2001**, *98*, 11857–11862.
(17) Han, T. H.; Kim, J.; Park, J. S.; Park, C. B.; Ihee, H.; Kim, S. O. *Adv. Mater. (Weinheim, Fed. Repub. Ger.)* **2007**, *19*, 3924–3927.
(18) Shen, C.-L.; Fitzgerald, M. C.; Murphy, R. M. *Biophys. J.* **1994**, *67*, 1238–1246.
(19) Soto, C.; Sigurdsson, E. M.; Morelli, L.; Kumar, R. A.; Castano, E. M.; Frangione, B. *Nat. Med.* **1998**, *4*, 822–826.
(20) Krysmann, M. J.; Castelletto, V.; Kelarakis, A.; Hamley, I. W.; Hule, R. A.; Pochan, D. J. *Biochemistry* **2008**, *47*, 4597–4605.

10.1021/la800942n CCC: $40.75
Published on Web 06/21/2008

Scheme 1. Molecular Structure of AAKLVFF

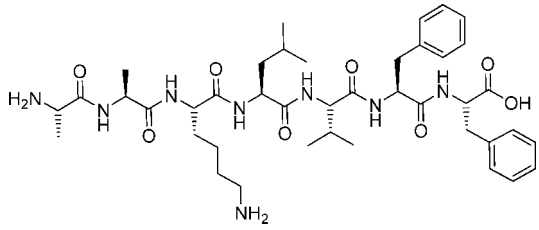

We have prepared variants of KLVFF extended at the N-terminus with additional hydrophobic residues with the aim to investigate the role of hydrophobic and aromatic interactions on peptide self-assembly. In particular, we have examined the fibrillization of FFKLVFF in methanol (the peptide is too hydrophobic to dissolve in water) and found evidence for β-sheet self-assembly.[21] We propose that this is driven in large part by aromatic interactions between F residues, as confirmed by UV (ultraviolet) and CD (circular dichroism) spectroscopy. A sample with nonaromatic residues at one terminus, AAKLVFF, was also prepared. This has solubility in both aqueous and nonaqueous solvents. The present paper presents unexpected results regarding its self-assembly in methanol. It is shown to self-assemble into nanotubes, which can form a nematic phase at sufficiently high concentration.

2. Experimental Section

Materials. AAKLVFF (Scheme 1) was synthesized by solid phase methods using standard FastMoc [Fmoc (9-fluorenylmethyloxycarbonyl) protecting group and activation by HBTU (2-(1*H*-benzotriazol-1-yl)-1,1,3,3-tetramethyluronium hexafluorophosphate)] chemistry. Amino acids [Fmoc-alanine-OH, Fmoc-lysine(Boc)-OH, Fmoc-leucine-OH, Fmoc-valine-OH, Fmoc-phenylalanine-OH], Fmoc-phenylalanine−Wang resin, and HBTU were purchased from Novabiochem. HOBt/DMF (a mixture of 1-hydroxybenzotriazole and dimethylformamide), DIEA/NMP (a mixture of diisopropylethylamine and *N*-methylpyrrolidone), and NMP were obtained from Applied Biosystems. Water (HPLC grade), acetonitrile (HPLC grade), acetic acid, and diethyl ether were purchased from Fluka. Piperidine, trifluoroacetic acid (TFA), triisopropylsilane, methanol, trifluoroethanol, and all other reagents were purchased from Sigma-Aldrich and were of the highest purity.

The peptide was synthesized on a 0.25 mmol scale using a fully automated peptide synthesizer (433A Applied Biosystems), which allowed for direct conductivity monitoring of Fmoc deprotection.

The resin used for AAKLVFF peptide synthesis was Fmoc-phenylalanine−Wang resin with 0.74 mmol g^{-1} substitution. The peptide was assembled from the C-terminus toward the N-terminus and was attached to the solid support at the C-terminus by the α-carbonyl group of the amino acid. According to the standard FastMoc protocol, the first step of the reaction was to remove the Fmoc protecting group from the amino acid using a solution of piperidine in NMP. The next step was activation of the carbonyl group of the new amino acid (dissolved in NMP) using HBTU (dissolved in HOBt, DIEA, and DMF). The activated amino acid was transferred from the activation vessel to the reaction vessel containing the previously deprotected amino terminal group of the peptide chain, and coupling was performed. To obtain the highest coupling efficiency, four times excess of each amino acid was used in 0.25 mmol cycles. Peptide attached to the solid support was obtained from the synthesizer. In the cleavage step, a mixture of 95% TFA, 2.5% triisopropylsilane, and 2.5% water was used. The sample was occasionally shaken at room temperature for approximately 4 h and the insoluble resin was washed with TFA. The peptide solution was precipitated in ice cold diethyl ether. Sample was separated by centrifugation and the solvent was decanted. The solid peptide was washed with diethyl ether and dried. During the cleavage the side chain protecting groups (Boc) were removed by TFA. The crude peptide was purified by reverse-phase high performance liquid chromatography (RP-HPLC; Perkin Elemer 200) using a C18 semipreparative column (Macherey-Nagel), for 30 min with flow rates 4 mL/min. A mobile phase of water and acetonitrile with 0.1% TFA was used. Sample elution was monitored by using a UV/vis detector operating at 220 nm. The sample dissolved in HPLC solvents was freeze-dried. Molecular weight was determined by electro-spray mass spectrometry.

The ^{1}H NMR spectra in methanol-d_4 were recorded using a Bruker AMX 400 instrument. The unambiguous assignments of proton shifts were made by homonuclear analysis (TOCSY) and comparison with KLVFF (data not presented).

^{1}H NMR (400 MHz methanol-d_4, ppm): 0.85 [2d, 6H, 2×CH_3 (Val) J = 6.72 Hz]; 0.94 [2d, 6H, 2×CH_3 (Leu) J = 6.50 Hz]; 1.32−1.95 [m, 15H, 4×CH_2 (Lys, Leu), CH (Leu), 2×CH_3 (Ala)]; 1.98−2.05 [m, 1H, CH (Val)]; 2.85−2.98 [m, 2H, CH_2 (Lys)]; 3.02−3.29 [m, 4H, CH_2 (Phe)]; 3.48−3.55 [m, 1H, CHα (Ala)]; 3.95−4.08 [m, 1H, CHα (Ala)]; 4.15 [d, 1H, CHα (Val) J = 7.36 Hz]; 4.38−4.42 [m, 1H, CHα (Lys)]; 4.45−4.52 [m, 1H, CHα (Leu)]; 4.65−4.74 [m, 2H, CHα (Phe)]; 7.21−7.33 [m, 10H, arom (Phe)]; 7.96, 8.09, 8.18, 8.21, 8.22, 8.23, 8.25, 8.61 [10H, NH, NH_2 (Ala, Lys, Leu, Val, Phe)].

Circular Dichroism. The circular dichroism (CD) spectra were recorded on a Chirascan spectropolarimeter (Applied Photophysics, UK). Samples were dissolved in methanol (0.03 wt %) and loaded into a 1 mm quartz cuvette. Spectra were obtained from 200 to 260 nm with a 0.5 nm step, 1 nm bandwidth, and 2 s collection time per step at 20 °C, taking five averages.

Fluorescence Spectroscopy. Spectra were measured on a Perkin Elementar Luminescence spectrometer (LS50B). Samples were contained in 1.0 cm path length quartz cuvettes. The fluorescence intensity was measured for methanol and AAKLVFF (0.02 wt %) in methanol by excitation at 265 nm (slit width 5 nm). The spectra were recorded from 270 to 450 nm, taking 20 averages at room temperature, and the background was subtracted.

UV/Visible Spectroscopy. A Chirascan spectropolarimeter was used in UV absorption mode, with the sample in a 1.0 cm quartz cuvette. The absorbance was measured for methanol and AAKLVFF (0.02 wt % in methanol). The spectra were recorded from 200 to 400 nm at room temperature, and the background was subtracted.

Fourier Transform Infrared Spectroscopy. IR spectra in the amide band regions were recorded on a FTIR spectrometer equipped with a DTGS detector. AAKLVFF solution in d_4-methanol (0.5, 1, and 2 wt %) was sandwiched between two CaF_2 plate windows (spacer 0.006 mm) and a solid film of dry peptide was deposited on one CaF_2 plate by drying the same solution. Spectra were scanned 64 times over the range of 4000−400 cm^{-1}. Spectral Manager for Windows was used for data acquisition and handling.

Electron Microscopy. TEM and ESEM were performed in the Centre for Advanced Microscopy at the University of Reading. A JEOL 2010 high-resolution transmission electron microscope (HR TEM), operated at 200 kV, was used to record images. A droplet of the sample (1 wt % in methanol) was placed on polyvinyl formal grids (Agar Scientific), stained with uranyl acetate (1 wt %) (Agar Scientific), and dried.

Polarized Optical Microscopy. A sample solution of AAKLVFF (1 wt % in methanol) was placed between crossed polarizers and images were obtained with an Olympus CX-41 microscope.

Dynamic Light Scattering (DLS). Dynamic light scattering measurements were carried out on well-filtered solutions by means of an ALV/CGS-3 compact goniometer system with ALV/LSE-5003 correlator using vertically polarized incident light of wavelength λ = 632.8 nm. Measurements were performed at an angle θ = 90° to the incident beam and data were collected three times for 30 s. The correlation functions (DLS) were analyzed by the constrained regularized CONTIN method[22,23] to obtain distributions of decay

(21) Krysmann, M. J.; Castelletto, V.; Hamley, I. W. *Soft Matter* **2007**, *3*, 1401–1406.

(22) Provencher, S. W. *Comput. Phys. Commun.* **1982**, *27*, 213.

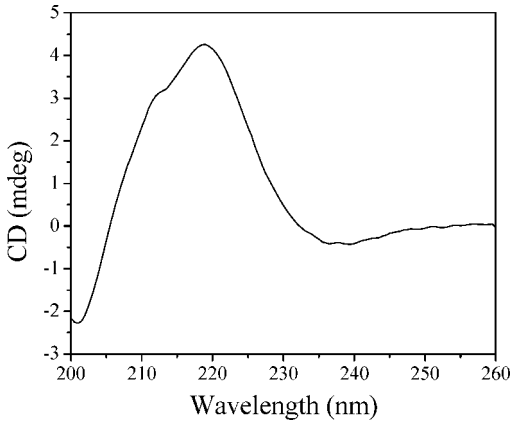

Figure 1. Circular dichroism spectrum of AAKLVFF in methanol (0.03 wt %).

rates (Γ) and hence distributions of the apparent mutual diffusion coefficient $D_{app} = \Gamma/q^2$ [$q = (4\pi n/\lambda)\sin(\theta/2)$, where n is the refractive index of the solvent], and ultimately distributions of the apparent hydrodynamic radius of the particle via the Stokes−Einstein equation

$$R_{h,app} = k_B T/(6\pi\eta D_{app}) \quad (1)$$

where k_B is the Boltzmann constant and η is the viscosity of the solvent at temperature T.

Small-Angle X-ray Scattering (SAXS). SAXS experiments were performed on beamline 2.1 at the SRS in Daresbury, United Kingdom. A 0.5 wt % sample in methanol was placed in a sealed cell in an O-ring between mica windows. Temperature control was achieved using a water bath. A gas-filled multiwire area detector was used to collect two-dimensional images that were reduced by radial integration to one-dimensional profiles. The sample−detector distance was 3.5 m. Subtraction of background scattering (methanol solvent) was performed for the data presented here.

Small Angle Neutron Scattering (SANS). SANS experiments were performed on the LOQ diffractometer at the ISIS spallation neutron source, Rutherford Appleton Laboratory, Didcot, UK. LOQ is a time-of-flight instrument that simultaneously uses a range of neutron wavelengths to cover a wide range of scattering vectors, q. In these experiments $0.07 \le q/\text{nm}^{-1} \le 2.9$, where $q = 4\pi\sin(\theta/2)/\lambda$, θ is the scattering angle, and λ is the neutron wavelength. Solutions (0.5 and 2.0 wt % peptide) in methanol-d_4 (to reduce background scattering and maximize the contrast with the hydrogeneous peptide) were filled in 1-mm standard quartz cuvettes (Hellma). Measurements were performed at room temperature. The SANS data were corrected for the measured sample transmission and background scattering (using methanol-d_4 as a reference). The data were collected using a two-dimensional area detector and reduced to a one-dimensional form by radial averaging, to produce intensity curves $I(q)$.

3. Results and Discussion

Secondary Structure. The secondary structure of peptide AAKLVFF was assessed using circular dichroism and UV absorption/fluorescence spectroscopy for dilute solutions and FTIR spectroscopy for more concentrated solutions and a dried film.

Figure 1 shows a CD spectrum for AAKLVFF in methanol solution. It was previously reported that CD spectra of short peptides, in which self-assembly is based on stacking interactions of aromatic units, show positive maxima at 200 and 218,[24] and indeed, we have observed this type of CD spectrum for KLVFF (in water or TFE)[20] and FFKLVFF (in methanol).[21] The CD spectrum obtained for AAKLVFF in methanol (Figure 1) seems

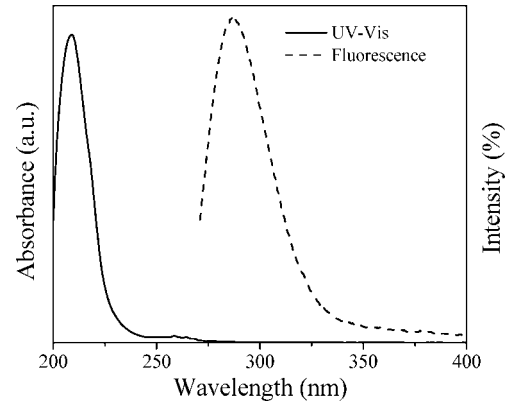

Figure 2. UV/visible absorption and fluorescence spectra showing aromatic interactions in AAKLVFF (0.02 wt % in methanol).

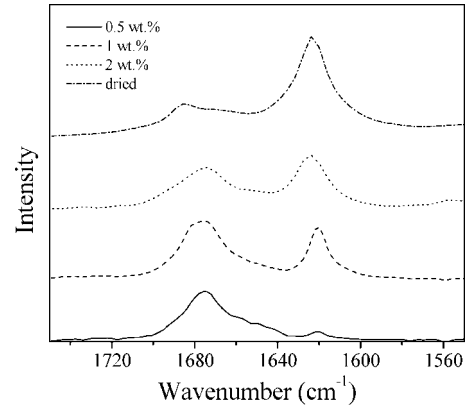

Figure 3. FTIR spectra of the amide I region of AAKLVFF in methanol-d_4 (0.5, 1, 2 wt %) and a dried film. The solvent spectrum has been subtracted from the spectra of the peptide solutions.

to be dominated by the maximum at 220 nm, although there is an extended shoulder at lower wavelengths.

Further evidence for aromatic interactions is provided by UV/visible fluorescence and absorption spectroscopy (Figure 2), performed for diluted samples. The fluorescence spectrum shows a peak at 290 nm that corresponds to $\pi-\pi^*$ stacking interactions of phenyl units. In the absorption spectrum, two peaks occur at 210 and 260 nm, the latter corresponding to that previously reported for F residues in proteins and the former also arising from phenyl rings.[25,26]

The main focus of the FTIR experiments was on the amide I band, which is sensitive to secondary structure. Additional peaks were located in the amide A band at 3278 cm^{-1} and amide B band at 3088 cm^{-1}. An absorption peak at 3030 cm^{-1} was due to the stretching vibration from the benzene rings. A peak at 2957 cm^{-1} was due to the CH_3 vibration. A peak at 2931 cm^{-1} was assigned to the CH_2 asymmetric stretching bands while a peak at 2874 cm^{-1} was due to the CH_3 symmetric stretching bands. The peaks at 1684 and 1623 cm^{-1} were assigned to the amide I band, and the peak at 1445 cm^{-1} was associated with the amide II band.[27,28]

FTIR spectra in the amide I region are shown in Figure 3 for solutions in methanol-d_4 and a dried film. In solution, two peaks

(23) Provencher, S. W. *Comput. Phys. Commun.* **1982**, *27*, 229.
(24) Gupta, M.; Bagaria, A.; Mishra, A.; Mathur, P.; Basu, A.; Ramakumar, S.; Chauhan, V. S. *Adv. Mater.* **2007**, *19*, 858–861.
(25) Kitagawa, T. *Prog. Biophys. Mol. Biol.* **1992**, *58*, 1–18.
(26) Schmid, F. X. In *Encyclopedia of Life Sciences*; Nature Publishing: London, 2001.
(27) Stuart, B. *Biological Applications of Infrared Spectroscopy*; Wiley: Chichester, 1997.
(28) Lin, S.-Y.; Chu, H.-L. *Int. J. Biol. Macromol.* **2003**, *32*, 173–177.

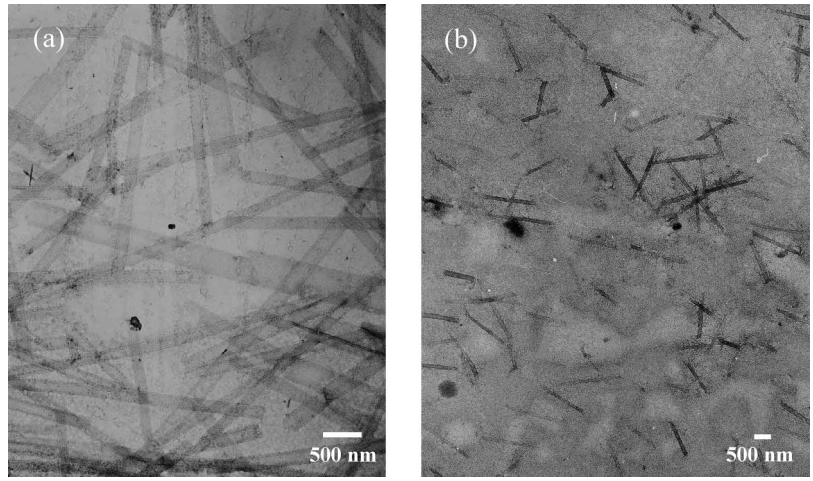

Figure 4. Transmission electron microscopy images of dried films of nanotubes prepared from 1 wt % solutions in methanol, staining with uranyl acetate. (a) High-resolution image of mature nanotubes. (b) Image of nanotubes at an early stage of growth.

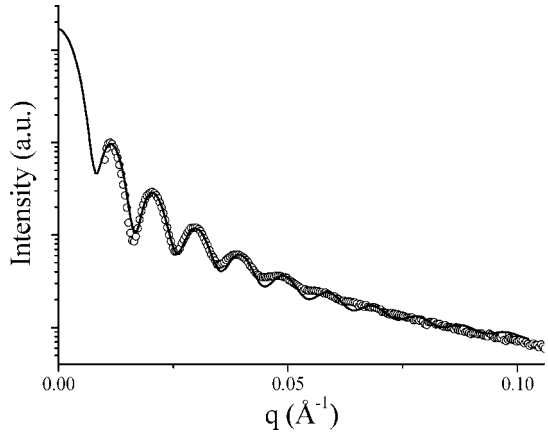

Figure 5. SAXS data (circles) for a 0.5 wt % peptide solution, with the model fit (line) described in the text.

at 1675 and 1620−1623 cm^{-1} were detected. These peaks are associated with a β-sheet structure.[27,29] It was observed that the absorbance of the peak at lower frequency (often associated with parallel β-sheets[27,29] increased with peptide concentration. The higher frequency peaks are often ascribed to an antiparallel β-sheet structure, although they could also be due to turns or bends. The ratio between those two peaks is different for solution and the dried film and suggests that the antiparallel β-sheet structure is favored in dilute solution and the parallel β-sheet structure in the dried film.

In summary, FTIR indicates a β-sheet secondary structure in the solution and solid samples. CD, UV/visible fluorescence, and absorption spectra are dominated by aromatic interactions.

Self-Organization. Transmission electron microscopy and small-angle X-ray scattering provide evidence for nanotube formation. Figure 4 contains TEM images for mature nanotubes (several days after the peptide was dissolved in methanol) and for shorter fibrils formed shortly after dissolution. The evolution of nanotube dimensions was studied also by dynamic light scattering, to be discussed shortly. The average width of the mature tubes (main population) is 116 ± 16 nm; the length is variable but exceeds 1 μm for all nanotubes. The early stage image (Figure 4b) indicates a tube width of 130 ± 26 nm and length of 1.4 ± 0.3 μm. The average tube width does not vary (outside the uncertainty) substantially when comparing the early stage and mature fibrils; however, there is a noticeable increase in length. This leads also to an increase in hydrodynamic radius, as probed by dynamic light scattering, discussed shortly. A further notable feature in the image for the mature fibril is the presence of an additional small fraction of fibrils with approximately twice the width of the majority population. This may result from a proportion of wider β-sheets.

SAXS provides in situ evidence for nanotube formation in solution. Figure 5 shows the SAXS profile obtained for a 0.5 wt % sample of mature fibrils. The scattering curve is dominated by the shape of the scattering particle, allowing the fitting of the SAXS curve using a form factor $P(q)$ for a suitable particle shape.

Several tests showed that the SAXS data in Figure 5 can be modeled according to the form factor of a hollow cylinder, with length L, internal polydisperse radius r_0 and external radius r_e:

$$P(q) = \int_0^\infty \int_0^1 e^{-(r-r_0)^2/2\sigma^2} \frac{1}{[1-(r_e/r)^2]} \left[\frac{J_1(qrX)}{qrX} - (r_e/r)^2 \frac{J_1(qr_eX)}{qr_eX} \right]^2 \left[\frac{\sin(qLY)}{(qLY)} \right]^2 dY\, dr \quad (2)$$

where $X = \sqrt{(1 - Y^2)}$, and the parameters obtained from the fit were r_e = 32.5 nm, L = 60 nm, r_0 = 36 nm, and σ = 41. The polydispersity in the internal radius r_0 of the hollow cylinder is 11%. It was found to be necessary to incorporate polydispersity to fit the SAXS data, in contrast to Lynn and co-workers, who used a monodisperse variant of eq 2 to fit SAXS and SANS data from their Aβ(16−22) nanotubes.[9]

The nanotube (external) diameter (d = 72 nm) obtained from SAXS is significantly smaller than the nanotube width obtained from TEM. This was previously noted by Lynn and co-workers for their KLVFFAE nanotubes.[9] They note that the structure imaged in TEM may be collapsed (unrolled) nanotubes, and allowing for the $2\pi r$ circumference of the tube, the corresponding flat fibril width using the radius from SAXS would be 113 nm, in excellent agreement with the value from TEM. Also following Lynn and co-workers, we can propose a model of the nanotube structure, based on geometrical relationships for winding of a tape into a helical ribbon developed by Chung et al.[30] The tendency for the β-sheets to twist into ribbons[31] results from the interfacial curvature with its origin in the packing of side chains with different

(29) Haris, P.; Chapman, D. *Biopolymers* **1995**, *37*, 251–263.

(30) Chung, D. S.; Benedek, G. B.; Konikoff, F. M.; Donovan, J. M. *Proc. Natl. Acad. Sci. U.S.A.* **1993**, *90*, 11341–11345.

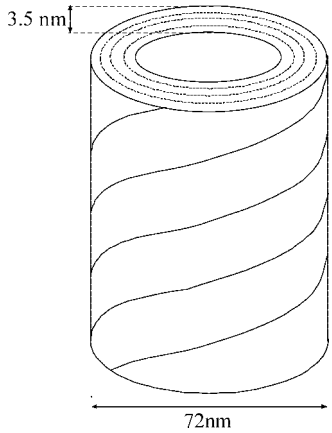

Figure 6. Model for nanotube structure, based on helical wrapping of a bilayer β-sheet into a tube.

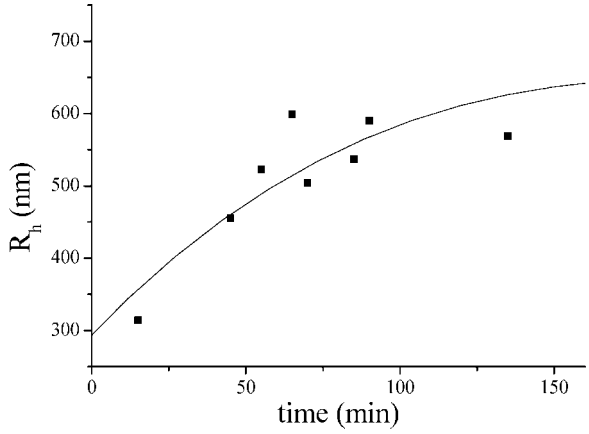

Figure 7. Evolution of the hydrodynamic radius obtained from dynamic light scattering experiments for a 1 wt % solution of AAKLVFF following dissolution in methanol. The line is a guide to the eye.

effective volumes (e.g., aromatic vs nonaromatic residues). The resulting model is sketched in Figure 6. The nanotube wall thickness from the SAXS model is 3.5 nm; this corresponds to approximately four stacked β sheets, with a sheet spacing of approximately 0.9 nm, as sketched in the figure.

A kinetic study based on particle dimensions from dynamic light scattering reveals a rapid self-assembly process of AAKLVFF which is stabilized after approximately 1 h (Figure 7). The particle dimensions obtained from analysis of correlation functions in dynamic light scattering using the Stokes−Einstein equation (eq 1) correspond to an effective isotropically averaged hydrodynamic radius, R_h. For a nonspherical particle, such as a nanotube, the interpretation of R_h is complex. However, approximating the tubes as rigid rods it has been reported that[32]

$$R_h \sim \frac{L}{2\ln(L/d)} \qquad (3)$$

Here L denotes the length of a rod and d its diameter. Taking values of L and d for short fibrils leads to $R_h = 295$ nm, in remarkably good agreement with the value measured by DLS (Figure 7).

Figure 8 shows a birefringent texture observed using polarized optical microscopy for a 1 wt % sample in methanol, indicating the formation of a nematic phase at higher concentration. Evidence for flow alignment of the nematic phase was also provided by

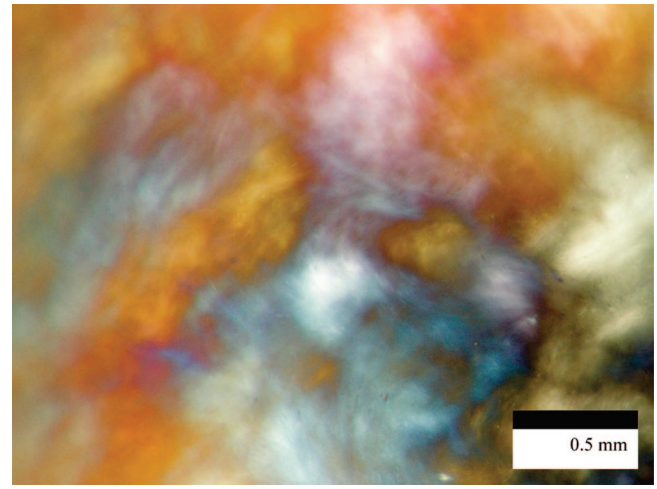

Figure 8. Polarized optical microscope image of the birefrigent texture of AAKLVFF (1 wt % methanol).

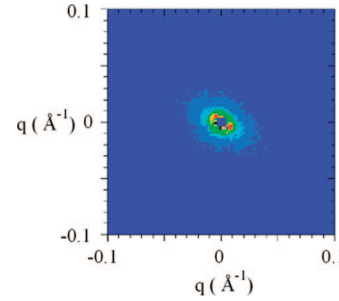

Figure 9. SANS data showing alignment of a 2 wt % solution of AAKLVFF in methanol-d_4.

small-angle neutron scattering. Figure 9 shows data obtained for a 2 wt % solution of mature fibrils in methanol-d_4. The elliptical intensity contours arise from aligned rodlike objects. Spontaneous alignment along an ill-defined flow direction was observed after pouring the sample into the cuvette. The alignment was retained for at least several hours between placing the sample in the cuvette and the SANS measurement. Further work is in progress to probe the flow-induced alignment of the nematic phase in more detail.

4. Summary

Our present study builds on our previous work with peptide FFKLVFF, which is too hydrophobic to dissolve in water but which forms fibrils in methanol.[21] AAKLVFF is soluble in both methanol and water. The present study is focused on self-assembly in methanol. It is remarkable that substitution of one of the FF residues with AA residues gives rise to a distinct motif, i.e. peptide nanotubes. These are quite clearly resolved through the combination of TEM and SAXS, in contrast to FFKLVFF in methanol, where both these techniques indicated the formation of (nonhollow) fibrils. The precise functionality at the nanotube surface is yet to be determined, but may be exploitable in future applications of our novel peptide nanotubes. The observation of a nematic phase at higher concentration of the nanotubes is also unprecedented, and this provides a means to fabricate oriented peptide-based structures with a diversity of potential uses.

Acknowledgment. We thank Dr. Rebecca Green (Dept of Pharmacy, University of Reading) for access to the FTIR instrument and Tina Geraki for assistance with SAXS experiments on station 2.1 at the SRS.

LA800942N

(31) Nyrkova, I. A.; Semenov, A. N.; Aggeli, A.; Bell, M.; Boden, N.; McLeish, T. C. B. *Eur. Phys. J. B* **2000**, *17*, 499–513.
(32) Riseman, J.; Kirkwood, J. G. *J. Chem. Phys.* **1950**, *18*, 512–516.